Available online at www.sciencedirect.com
ScienceDirect
Ceramics International 36 (2010) 1743–1747
CERAMICS INTERNATIONAL
www.elsevier.com/locate/ceramint

Short communication

Surface morphology and conductivity of zirconium-doped nanostructured indium oxide films with various crystallographic features

Yuan-Chang Liang *

Institute of Materials Engineering, National Taiwan Ocean University, No. 2, Peining Rd., Keelung City 20224, Taiwan

Received 11 February 2010; received in revised form 15 February 2010; accepted 1 March 2010
Available online 24 April 2010

Abstract

Zr-doped In_2O_3 (Zr-In_2O_3) thin films with various degrees of crystallography ((2 2 2)-epitaxial, (2 2 2)-textured, and randomly oriented films) were grown on various substrates by rf magnetron sputtering. Atomic force microscopy images demonstrate that the substrate profoundly affects the topography of the Zr-In_2O_3 films. The surface of the Zr-In_2O_3 epilayer on the Al_2O_3(0 0 0 1) substrate comprises a three-dimensional island-like structure. Some discrete mounds were found on the Zr-In_2O_3 film grown on the ZnO(0 0 2)-buffered Al_2O_3(0 0 0 1) substrate. Large triangular grains contribute to the largest root mean square surface roughness of the polycrystalline Zr-In_2O_3 film on the Si(1 0 0) substrate. Current maps obtained by conductive atomic force microscopy show that the current distribution depends on the surface topography. Comparatively, the surface of the Zr-In_2O_3 epilayer on the Al_2O_3(0 0 0 1) substrate exhibits a smooth feature, and the corresponding spatial distribution of current images reveals a more homogeneous current map than that of the textured and polycrystalline films.

Keywords: A. Films; B. Non-destructive evaluation; E. Electrodes

1. Introduction

Transparent conducting oxides (TCOs) are extensively used as transparent electrodes in various optoelectronic devices due to their unique optical and electrical properties [1–4]. A great number of TCO thin films have been extensively investigated recently [5–7]. Among TCOs, indium oxide (In_2O_3), a wide band gap semiconductor, is known as the most common optically transparent electronic conductor. Recently, the improvement of the optoelectronic properties of In_2O_3 was realized by doping with higher valence cations [1,6]. Most studies of the structural characteristics of impurity-doped In_2O_3 films have focused on the effects of process conditions [6,8]. However, understanding the surface morphology of this class of materials depends on characterizing the growth of a film on various substrates. Studies on the physical properties of heteroepitaxial Sn-doped In_2O_3 films on single crystal substrates and polycrystalline In_2O_3 thin films with mixed crystallographic orientations have been undertaken [6,9,10]. However, research is continuing to improve their physical properties for practical applications. Till now, no conclusive study of the effects of the substrate on the surface morphology for a particular crystallographic orientation under identical process conditions and on the properties of In_2O_3 films is available. In particular, understanding of the local structure and electrical properties of such films on the nanometer scale is lacking. This is a crucial issue for TCO films being used as contact electrode for nanodevices. Conductive atomic force microscopy enables the electrical properties to be correlated with the surface topography on the nanometer scale, and this technique has been applied to semiconductor hetero-structures [11]. The crystallographic effects on the surface morphology and nanostructural conductive properties of zirconium-doped indium oxide films that originate in different substrates are reported in this work.

2. Experimental

Zr-doped In_2O_3 (Zr-In_2O_3) films were grown on Al_2O_3(0 0 0 1), ZnO(0 0 2)-coated Al_2O_3(0 0 0 1), and Si(1 0 0) substrates using rf magnetron sputtering. The target adopted in the experiment was prepared by mixing the 5 wt%

* Tel.: +886 2 24622192; fax: +886 2 24625324.
E-mail address: yuanvictory@gmail.com.

0272-8842/$36.00
doi:10.1016/j.ceramint.2010.03.004

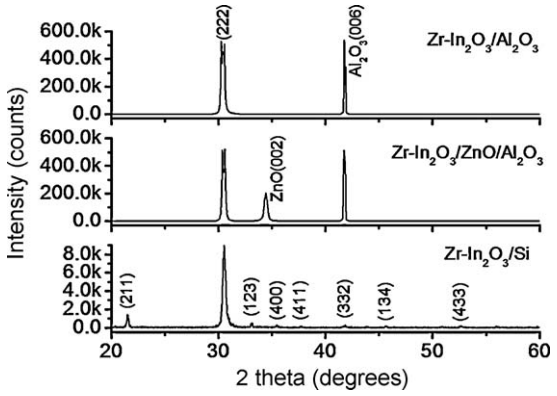

Fig. 1. XRD patterns of the Zr-In_2O_3 films on various substrates.

ZrO_2 and 95 wt% In_2O_3 precursor oxide powders, pressing the powders into pellets, followed by sintering to high density. The thickness of the Zr-In_2O_3 is fixed at about 210 nm. The thickness of the ZnO buffer layer is ~100 nm. The growth temperature of the Zr-In_2O_3 and ZnO films was kept at 350 °C. The gas pressure of deposition for Zr-In_2O_3 films was fixed at 5 mTorr with a pure Ar atmosphere. The gas pressure of deposition was fixed at 5 mTorr with an Ar/O_2 ratio of 4:1 for the ZnO buffer layer. The atomic percentages of the as-deposited films are calculated from the X-ray photoelectron spectroscopy (XPS) spectra of Zr3d, In3d5 and O1s regions.

The crystallographic structures of the Zr-In_2O_3 films were analyzed by X-ray diffraction (XRD). The surface morphology of the Zr-In_2O_3 films was investigated by atomic force microscopy (AFM). The cross-section image of the Zr-In_2O_3/ZnO-coated Al_2O_3(0 0 0 1) was investigated using transmission electron microscopy (TEM). The surface current images of the Zr-In_2O_3 films were also observed using Conductive atomic force microscopy (CAFM) with PtIr tips.

3. Results and discussion

Fig. 1 presents the Zr-In_2O_3 films with intense (2 2 2) Bragg reflections on the Al_2O_3(0 0 0 1) and ZnO-coated Al_2O_3(0 0 0 1) substrates. The absence of ZrO_2 phase in the XRD patterns indicates a good solid solution of Zr in the In_2O_3 films. The ZnO buffer layer is orientated such that its (0 0 2) direction is parallel to the (0 0 0 1) direction of Al_2O_3. Yi et al. [12] proposed the planes of bixbyite In_2O_3 and wurtzite ZnO with the most densely packed oxygen to be parallel to (2 2 2) and (0 0 2), respectively, suggesting that the ZnO(0 0 2) buffer-layer provides a good template for the growth of In_2O_3(2 2 2) films. The phi-scans of the Zr-In_2O_3(0 0 4) Bragg reflections show a clear sixfold rotational symmetry of the Al_2O_3(0 0 0 1) substrate (not shown here), revealing excellent in-plane crystalline orientation of the Zr-In_2O_3 film on Al_2O_3(0 0 0 1) substrate. However, no Zr-In_2O_3(0 0 4) Bragg reflection was detected showing that the Zr-In_2O_3 films grown on the ZnO-coated Al_2O_3(0 0 0 1) are polycrystalline with a preferred (2 2 2) orientation. Moreover, the Zr-In_2O_3 films grown on the Si(1 0 0) substrates are polycrystalline and yield various Bragg reflections, which correspond to the cubic bixbyite In_2O_3 phase [8].

Wide scan XPS spectra of the Zr-In_2O_3 films grown on various substrates are presented in Fig. 2(a) which shows four major peaks corresponding to zirconium (Zr3d and Zr3p), indium (In3d) and oxygen (O1s). The atomic percentages of the films are calculated from the narrow scan XPS spectra of Zr3d, In3d5 and O1s regions. Moreover, the dependence of the O1s peak of the Zr-In_2O_3 films on the various substrates can be observed on the Gaussian-resolved results in Fig. 2(b)–(d). The lower binding energy O1s component (at ~530.3 eV) is attributed to oxygen in the oxide crystal and the higher binding energy O1s component (at 531.2 eV) represents the oxygen

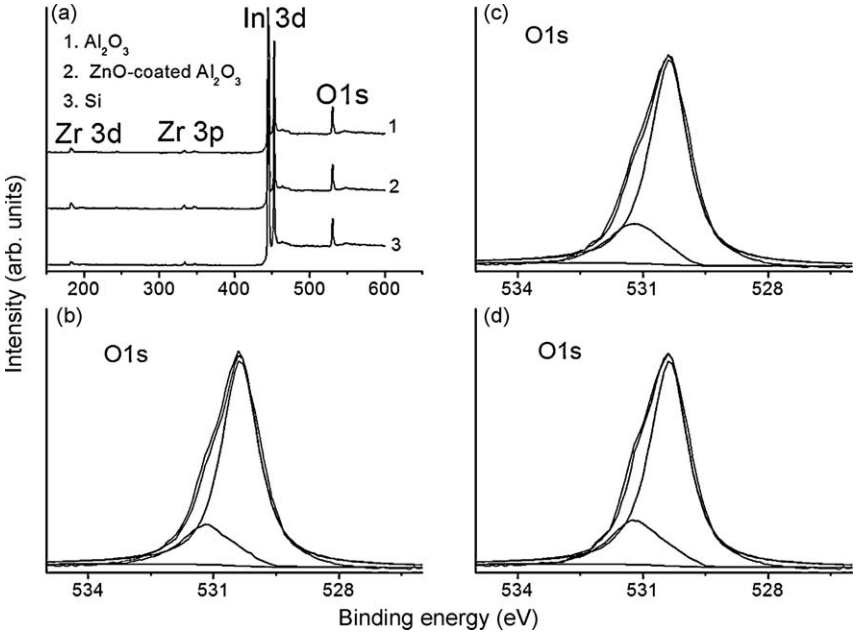

Fig. 2. (a) Wide scan XPS spectra of the Zr-In_2O_3 films grown on various substrates, (b) O1s peak of Zr-In_2O_3/Al_2O_3(0 0 0 1), (c) O1s peak of Zr-In_2O_3/ZnO(0 0 2)-buffered Al_2O_3(0 0 0 1), and (d) O1s peak of Zr-In_2O_3/Si(1 0 0).

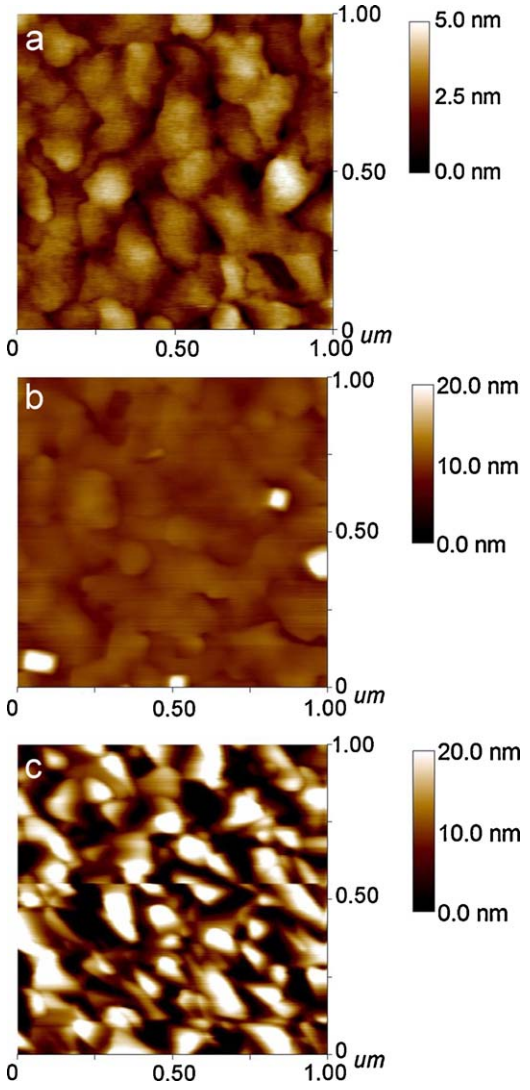

Fig. 3. Surface topography of the Zr-In_2O_3 films grown on various substrates. (a) Al_2O_3(0 0 0 1), (b) ZnO(0 0 2)-buffered Al_2O_3(0 0 0 1), and (c) Si(1 0 0).

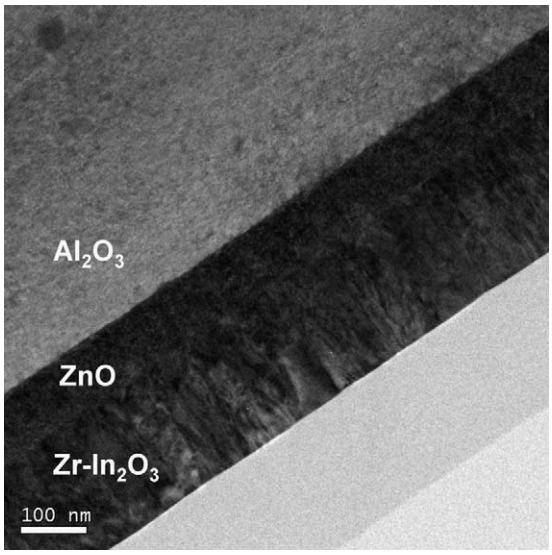

Fig. 4. Cross-sectional TEM image of the Zr-In_2O_3 film on ZnO(0 0 2)-buffered Al_2O_3(0 0 0 1).

ions in the oxygen-deficient regions. The films have a composition of $In_{1.89}Zr_{0.11}O_{2.37}$, $In_{1.89}Zr_{0.11}O_{2.35}$, and $In_{1.89}Zr_{0.11}O_{2.37}$ for Zr-In_2O_3/Al_2O_3(0 0 0 1), Zr-In_2O_3/ZnO-coated Al_2O_3(0 0 0 1), and Zr-In_2O_3/Si(1 0 0) films, respectively. These films have nearly the same oxygen content which deviates from the stoichiometric value. The cause of the non-stoichiometry of the oxygen content herein may arise from the deposition of the film in an oxygen deficient atmosphere [6].

The surface of the Zr-In_2O_3 epilayer on the Al_2O_3 substrate comprises a three-dimensional (3D) island-like structure with an root mean square (rms) surface roughness of 0.75 nm (Fig. 3(a)). The large mismatch (−13.2%) between In_2O_3(2 2 2) and Al_2O_3(0 0 0 1) results in a transition from two-dimensional to 3D growth when the growth thickness of In_2O_3 exceeded one monolayer [13]. Accordingly, the Zr-In_2O_3 film growth proceeds in an incoherent mode, developing 3D features. A surface undulation that develops to relieve strain under a large lattice misfit is observed in most heteroepitaxy systems [14,15]. The relatively rough surface of the Zr-In_2O_3 film on the ZnO-buffered Al_2O_3 substrate exhibits some protrusions, as shown in Fig. 3(b). The AFM surface structure herein is similar to the finding of Bourlange et al. [16]. The mechanism for the formation of discrete mounds herein might differ from that of the literature (high process temperature above 750 °C using MBE). Further investigation is needed to clarify the cause of discrete mounds formed on the Zr-In_2O_3/ZnO-buffered Al_2O_3 film. These mounds are much higher than the features observed on the film grown on a plain Al_2O_3 substrate. The film surface is rougher than the film grown on plain Al_2O_3 substrate, with an rms roughness of 1.56 nm. The mismatch between the average O–O distance of the crystallographic plane In_2O_3(2 2 2) and that in the ZnO(0 0 2) plane is 3%, which is far below the value associated with heteroepitaxial In_2O_3(2 2 2)/Al_2O_3(0 0 0 1). However, the surface roughness of the Zr-In_2O_3 film on the ZnO-buffered Al_2O_3 is almost twice that of the film on the Al_2O_3 substrate. Lattice mismatch may not the main cause of the aforementioned phenomenon. The surface roughness of the plain Al_2O_3 substrate is ∼0.45 nm. The rms surface roughness of the ZnO buffer layer on the Al_2O_3 substrate is 0.87 nm. The buffer layer may be responsible for a relatively large geometrical shadowing effect during the film growth, which further roughens the as-deposited film surface [17]. Moreover, the TEM image (Fig. 4) shows a clear columnar structure of the Zr-In_2O_3 film on the ZnO-buffered Al_2O_3. It was assumed that surface mobility of adatoms was limited by the grain boundaries of the ZnO buffer layer. This further induced the coalescence of individual smaller nuclei along the (2 2 2) orientation in which the crystallites may possess lower surface energy at the surface of the ZnO-buffered Al_2O_3 substrate. These columnar grains might also account for the higher surface roughness of the (2 2 2)-textured Zr-In_2O_3 film compared to the Zr-In_2O_3 epitaxy. The surface of the polycrystalline Zr-In_2O_3 film on the Si(1 0 0) substrate consists mainly of triangular grains (Fig. 3(c)) whose height can reach ∼40 nm, as determined by section analysis. Polycrystalline

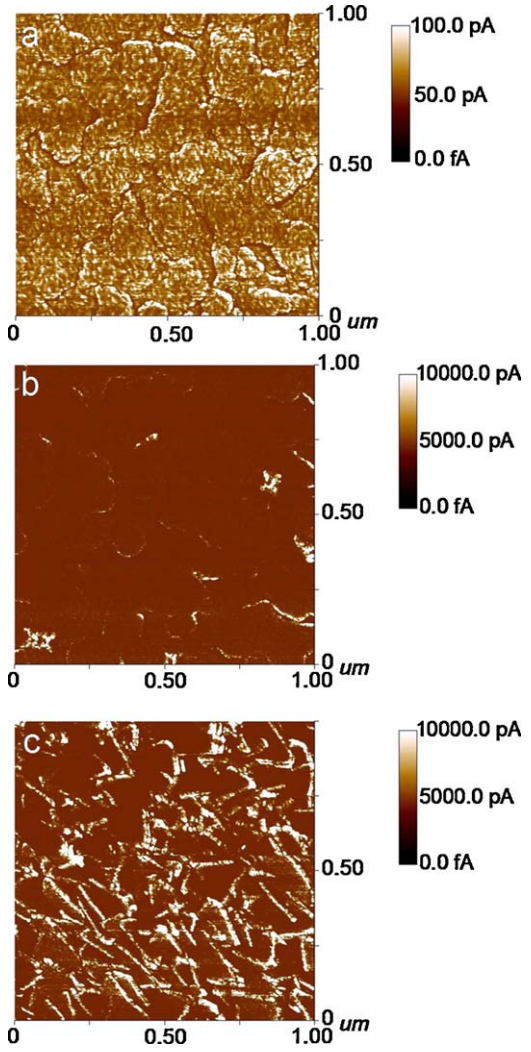

Fig. 5. The corresponding current images from Fig. 3. (a) Al_2O_3(0 0 0 1), (b) ZnO(0 0 2)-buffered Al_2O_3(0 0 0 1), and (c) Si(1 0 0).

Sn-doped In_2O_3 films sputtered on glass substrates have multi-shaped surface features. The grains of sputtered Sn-doped In_2O_3 films with ⟨4 0 0⟩ axes normal to the substrate surface are square and those with ⟨2 2 2⟩ and ⟨4 4 0⟩ axes are triangular and rectangular shapes, respectively [18]. However, the intensity ratios of the crystallographic planes (4 0 0)/(2 2 2) and (4 4 0)/(2 2 2), calculated from XRD are ∼3 and 1.6%, respectively, which are far below the values derived from the standard In_2O_3 samples (29.2 and 32.5% for (4 0 0)/(2 2 2) and (4 4 0)/(2 2 2), respectively, JCPDS no. 89-4595). In the present work, the crystallographic plane of (2 2 2) dominates the lattice characteristics of the sputtered deposited Zr-In_2O_3 film in an Ar atmosphere on the Si substrate. Large triangular grains contribute to the largest rms surface roughness, 4.76 nm, among all the samples.

Fig. 5 shows the current image at an applied bias during AFM scanning (the corresponding AFM images were shown in Fig. 3), which reflects the local nanostructural conductivity of the films. The surface of the Zr-In_2O_3 epilayer on the Al_2O_3 substrate exhibits a smooth feature, and the corresponding current image in Fig. 5(a) reveals a more homogeneous current map than for the films on the other substrates. Furthermore, a trace of the enhanced current conductions at the edges of the surface grains was found. The Zr-In_2O_3 film on the ZnO-buffered Al_2O_3 substrate, however, is associated with a wide range of variation of the current in the conducting region, suggesting that the conducting property is localized. Structural information reveals large currents in large crystallites that protrude from the surface. Enhanced current conduction at the edges of the grains was also observed in the film surface. The high protrusions exhibit a much larger current conduction than the relatively planar regions. These protrusions constitute a highly conductive path on the film. The current image of the polycrystalline Zr-In_2O_3 on the Si substrate is a high contrast map, as shown in Fig. 5(c). A highly nonhomogeneous current distribution was thus observed. The edges of the triangular grains conduct a large current with respect to that of the matrix. Most high currents are detected along the edges of prominent features, indicating that the crystallographic planes at such locations are more electrically active than other planes in the matrix. Similarly, an enhanced conduction inhomogeneity has been measured in amorphous $HfAlO_x$ films upon annealing at high temperatures, which also has been attributed to the formation of polycrystalline structures [19]. The hexagonal island surface feature of an as-grown GaN film is also associated with increased conduction in the island sidewalls [11]. The randomly oriented Zr-In_2O_3 film on the Si substrate clearly yields a markedly nonhomogeneous current map; this might further deteriorate the reliability of nanodevices when Zr-In_2O_3/Si is used as contact electrode.

4. Conclusions

Zr-In_2O_3 films with various degrees of crystallography were grown on Al_2O_3(0 0 0 1), ZnO-buffered Al_2O_3(0 0 0 1), and Si(1 0 0) substrates by rf magnetron sputtering. The Zr-In_2O_3 film on the Si(1 0 0) substrate has a polycrystalline structure with mixed crystallographic orientations. The large mismatch between the Zr-In_2O_3 film and the Al_2O_3(0 0 0 1) is responsible for the 3D island-like feature of the epilayer. The ZnO buffer layer on the Al_2O_3(0 0 0 1) substrate might further roughen the as-deposited Zr-In_2O_3 film. The polycrystalline Zr-In_2O_3 film has the largest rms surface roughness of the systems of interest. Comparatively, the Zr-In_2O_3 epilayer on the Al_2O_3(0 0 0 1) substrate exhibits a more homogeneous current map as required for use as contact electrode for optoelectronic nanodevices.

References

[1] Y.C. Liang, Y.C. Liang, Buffering effect on physical properties of transparent $BaTiO_3$ capacitors on composite transparent electrodes, Scr. Mater. 61 (2009) 117–120.
[2] Y.C. Liang, C.C. Liu, C.C. Kuo, Y.C. Liang, Structural and opto-electronic properties of transparent conducting (2 2 2)-textured Zr-doped In_2O_3/ZnO bilayer films, J. Cryst. Growth 310 (2008) 3741–3745.
[3] C.C. Liu, Y.C. Liang, C.C. Kuo, Y.Y. Liou, J.W. Chen, C.C. Lin, Fabrication and opto-electric properties of ITO/ZnO bilayer films on

polyethersulfone substrates by ion beam-assisted evaporation, Solar Energy Mater. Solar Cells 93 (2009) 267–272.
[4] N. Raghu, T.R.N. Kutty, Relationship between nonlinear resistivity and the varistor forming mechanism in ZnO ceramics, Appl. Phys. Lett. 60 (1992) 100–102.
[5] H.M. Zhou, D.Q. Yi, Z.M. Yu, L.R. Xiao, J. Li, Preparation of aluminum doped zinc oxide films and the study of their microstructure, electrical and optical properties, Thin Solid Films 515 (2007) 6909–6914.
[6] Y.C Liang, Y.C. Liang, Physical properties of low temperature sputtering-deposited zirconium-doped indium oxide films at various oxygen partial pressures, Appl. Phys. A: Mater. Sci. Process. 97 (2009) 249–255.
[7] D.H. Kim, N.G. Cho, H.G. Kim, W.Y. Cho, Structural and electrical properties of indium doped ZnO thin films fabricated by RF magnetron sputtering, J. Electrochem. Soc. 154 (2007) H939–H943.
[8] A.V. Mudryi, A.V. Ivaniukovich, A.G. Ulyashin, Deposition by magnetron sputtering and characterization of indium tin oxide thin films, Thin Solid Films 515 (2007) 6489–6492.
[9] N. Taga, H. Odaka, Y. Shigesato, I. Yasui, M. Kamei, Electrical properties of heteroepitaxial grown tin-doped indium oxide films, J. Appl. Phys. 80 (1996) 978–984.
[10] S. Kaleemulla, A. Sivasankar Reddy, S. Uthanna, P. Sreedhara Reddy, Physical properties of flash evaporated In_2O_3 films prepared at different substrate temperatures, Mater. Lett. 61 (2007) 4309–4313.
[11] J.W.P. Hsu, M.J. Manfra, D.V. Lang, S. Richter, S.N.G. Chu, A.M. Sergent, R.N. Kleiman, L.N. Pfeiffer, R.J. Molnar, Inhomogeneous spatial distribution of reverse bias leakage in GaN Schottky diodes, Appl. Phys. Lett. 78 (2001) 1685–1687.
[12] C.H. Yi, I. Yasui, Y. Shigesato, Oriented tin-doped indium oxide films on ⟨0 0 1⟩ preferred oriented polycrystalline ZnO films, Jpn. J. Appl. Phys. 34 (1995) 1638–1642.
[13] Z.X. Mei, Y. Wang, X.L. Du, Z.Q. Zeng, M.J. Ying, H. Zheng, J.F. Jia, Q.K. Xue, Z. Zhang, Growth of In_2O_3 single-crystalline film on sapphire (0 0 0 1) substrate by molecular beam epitaxy, J. Cryst. Growth 289 (2006) 686–689.
[14] Y.C. Liang, Y.C. Liang, Quantifying strain effects on physical properties of $La_{0.68}Ba_{0.32}MnO_3$ epilayers and heterostructures, J. Electrochem. Soc. 154 (2007) P147–P151.
[15] Y.C. Liang, Y.C. Liang, Strain-dependent surface evolution and magneto-transport properties of $La_{0.7}Sr_{0.3}MnO_3$ epilayers on $SrTiO_3$ substrates, J. Cryst. Growth 304 (2007) 275–280.
[16] A. Bourlange, D.J. Payne, R.G. Palgrave, J.S. Foord, R.G. Egdell, R.M.J. Jacobs, A. Schertel, J.L. Hutchison, P.J. Dobson, Investigation of the growth of In_2O_3 on Y-stabilized ZrO_2(1 0 0) by oxygen plasma assisted molecular beam epitaxy, Thin Solid Films 517 (2009) 4286–4294.
[17] R.P. Karunasiri, R. Bruinsma, J. Rudnick, Thin-film growth and the shadow instability, Phys. Rev. Lett. 62 (1989) 788–791.
[18] M. Kamei, Y. Shigesato, S. Takaki, Origin of characteristic grain–subgrain structure of tin-doped indium oxide films, Thin Solid Films 259 (1995) 38–45.
[19] X. Blasco, J. Pétry, M. Nafría, X. Aymerich, O. Richard, W. Vandervorst, C-AFM characterization of the dependence of $HfAlO_x$ electrical behavior on post-deposition annealing temperature, Microelectron. Eng. 72 (2004) 191–196.